Journal of Organometallic Chemistry 694 (2009) 2777–2785

Contents lists available at ScienceDirect

Journal of Organometallic Chemistry

journal homepage: www.elsevier.com/locate/jorganchem

Synthesis, characterization and electrophosphorescent properties of mononuclear platinum(II) complexes based on 2-phenylbenzoimidazole derivatives

Hui Li [a,b], Junqiao Ding [a], Zhiyuan Xie [a], Yanxiang Cheng [a,*], Lixiang Wang [a]

[a] State Key Laboratory of Polymer Physics and Chemistry, Changchun Institute of Applied Chemistry, Chinese Academy of Sciences, 5625 Renmin Street, Changchun, Jilin Province 130022, PR China
[b] Graduate School of Chinese Academy of Sciences, Beijing 100039, PR China

ARTICLE INFO

Article history:
Received 26 February 2009
Received in revised form 20 April 2009
Accepted 20 April 2009
Available online 3 May 2009

Keywords:
Platinum
2-Phenylbenzoimidazole
Phosphorescence
Spin-coating
Organic light-emitting diode

ABSTRACT

The rational design, synthesis and characterization of five phosphorescent platinum complexes [(C^N)Pt(acac)] [Hacac = acetylacetone, HC^N = 1-methyl-2-(4-fluorophenyl)benzoimidazole (H-FMBI), 1-methyl-2-phenylbenzoimidazole (H-MBI), 1,2-diphenyl-benzoimidazole (H-PBI), 1-(4-(3,6-di-*t*-butylcarbazol-9-yl))phenyl-2-phenylbenzoimidazole (*t*-BuCz-H-PBI), and 1-(4-(3,6-di-(3,6-di-*t*-butyl-carbazol-9-yl))carbazol-9-yl)phenyl-2-phenylbenzoimidazole (*t*-BuCzCz-H-PBI)] have been discussed. The crystal structure of (MBI)Pt(acac) shows a nearly ideal square planar geometry around Pt atom and the weak intermolecular interactions with π–π spacing of 3.55 Å. All of the complexes emit green phosphorescence from the metal-to-ligand charge-transfer (MLCT) excited state with high quantum efficiency (0.08–0.17) at room temperature. A multilayer organic light-emitting diode (OLED) with (MBI)Pt(acac) as phosphorescent dopant was fabricated using the method of high-vacuum thermal evaporation, which gives a maximum brightness, luminous and power efficiency of 13 605 cd/m^2, 15.1 cd/A and 4.3 lm/W, respectively. In contrast, the comparable performance can be achieved in the solution-processed OLED based on (*t*-BuCzPBI)Pt(acac) with a peak brightness, luminous and power efficiency of 13 606 cd/m^2, 17.5 cd/A and 8.4 lm/W, respectively. The better device efficiency results from the good square plane of central Pt coordination unit and the inhibition of the aggregates due to bulky and rigid *t*-butylcarbazole dendrons.

1. Introduction

Recently, square planar platinum(II) complexes have attracted intensive interest for their potential application in different fields such as chemical sensors [1,2], photovoltaic devices [3,4], emissive probes for DNA [5], and especially organic light-emitting diodes (OLEDs) [6–11]. Since the first report of the phosphorescent platinum(II) complex (PtOEP) in 1998 [12], a breakthrough using platinum(II) complex as efficient electroluminescent materials has been demonstrated, and a series of platinum(II) complexes, based on N^N [13,14], C^N [15–20], N^O [21], N^N^N [22,23], C^N^N [24–31], O^N^N [32] aromatic chelating ligands, have been synthesized one after the other. For example, the green emitting device using [**L**Pt(OPh)] [H**L** = 3,5-di(2-pyridinyl)toluene] displays a very high external quantum efficiency (EQE) of 16.5% and a reasonable operational stability [33]. Jabbour and Li's group offered a novel Pt complex [Pt-4, (1,3-difluoro-4,6-di(2-pyridinyl)benzene) platinum chloride], which shows a peak EQE of 16% for blue OLED and 9.3% for single-dopant white OLED, respectively [34].

However, the device stability and efficiency of a majority of platinum(II) complexes are still very low. For the sake of improving the device performance, two key issues may be considered. Firstly, keeping ideal coordination geometry of square plane of Pt atom, which can decrease the probability of metal-centered (d–d) states non-radiative deactivation and provide the emissive decay state at room temperature [35–37]. Che's group exploited the (C^N^N) cyclometalated ligands that show a strong preference for a planar geometry, and can therefore be expected to disfavor the excited-state distortion and promote radiative decay [38]. These platinum (II) complexes obtained have high phosphorescence quantum yields ranging from 0.21 to 0.68 in solutions at room temperature [37,39]. Secondly, restraining the formation of the aggregates and excimers [40] of the square planar molecular configuration of platinum(II) complexes. It seems contrary to the first, in fact, the worry has been solved by Chi and co-workers [41]. They choose a bulky, rigid camphor-like architecture ligand to effectively suppress the aggregation effect and drastically reduce the phosphorescence radiative lifetime to several microseconds. Consequently, highly efficient OLEDs operating at 610–630 nm have been successfully prepared with the corresponding platinum(II) complexes as dopants. In addition, using bi-, tri- or tetra-nuclear platinum(II)

* Corresponding author. Tel.: +86 431 85262106; fax: +86 431 85684937.
E-mail address: yanxiang@ciac.jl.cn (Y. Cheng).

0022-328X/$ - see front matter © 2009 Elsevier B.V. All rights reserved.
doi:10.1016/j.jorganchem.2009.04.024

complexes possessing three dimension geometry can act as the similar role, or realize intramolecular interaction rather than intermolecular interaction [42–45]. However, few successful examples mean that tremendous efforts still need to be made in the development of highly efficient phosphorescent platinum(II) complexes.

In our previous work, a class of C^N ligands based on 2-phenylbenzoimidazole has been applied successfully in cyclometalated iridium(III) complexes as high efficiency non-doped emitting materials [46], which impels us to synthesize corresponding phosphorescent platinum(II) complexes. This kind of C^N aromatic chelating ligands retains the metal-centered (MC) states of platinum(II) complexes to lie at higher energy than the intraligand and MLCT states, an advantageous situation for enhancing luminous efficiency. In other words, they can satisfy the demand of geometry of square planar platinum(II) complexes and simultaneously keep high phosphorescence quantum yields at room temperature. In addition, the bulky and rigid carbazole-based dendrons can be introduced conveniently to the periphery of this ligand, which can restrain the aggregates and excimers formation and further improve luminous efficiency. In fact, the performances of the OLEDs fabricated by solution process are comparable to those of high-vacuum thermal evaporation. The maximum luminous efficiency of 15.6 cd/A for the evaporation device of (MBI)Pt(acac) and 17.5 cd/A for the solution-processed device of (*t*-BuCzPBI)Pt(acac) are realized.

2. Result and discussion

2.1. Synthesis and structural characterization

The synthesis and chemical structure of the platinum(II) complexes are shown in Scheme 1. The synthetic routes are mature and general, which can be divided into two steps: first, the platinum salt reacts with the HC^N ligand and forms the chloride-bridged dimer, (C^N)Pt(μ-Cl)$_2$Pt(C^N). Then the dimer is cleaved with the acetyl acetone to give the corresponding monomeric (C^N)Pt(acac) complexes with moderate yield except (FMBI)Pt(acac) due to the presence of electron-withdrawing fluorine atom. All of the (C^N)Pt(acac) complexes were verified with ^{1}H and ^{13}C NMR spectroscopy, elemental analysis, and matrix-assisted laser desorption/ionization time-of-flight (MALDI-TOF) mass spectra. All the complexes are thermally stable up to 320 °C, as determined by thermal gravimetric analysis (TGA), which is beneficial to the long-term stability of OLEDs fabricated with these materials. The favorable solubility and air stability of them allow for all kinds of measurements.

X-ray single crystal structure analysis of (MBI)Pt(acac) was carried out and its crystal structure and molecular packing diagram are shown in Fig. 1. Selected bond lengths and angles are listed in Table 1. The bond distances of Pt–C [1.973(1)], Pt–N [2.000(1)] and Pt–O [1.990(9) and 2.049(9) Å] are similar to the mean value reported in the literature [47–50]. The bond angles of C(1)–Pt–O(1) [91.7(4)], C(1)–Pt–N(1) [80.1(4)], O(1)–Pt–O(2) [92.5(4)] and N(1)–Pt–O(2) [95.7(4)°] are typical for cyclometalates and β-diketonate derivatives of platinium(II) complexes [28]. The dihedral angle is only 5.0° between the planes of PtC1C6C7N1 and PtO1O2C16C17C18, which indicates that the molecule of (MBI)Pt(acac) has a nearly ideal square planar geometry. Moreover, benzoimidazole and phenyl rings also exhibit perfect planar geometry (the torsion angle of C1–C6–C7–N2, 2.27°) owing to bonding with Pt(II) atom. So we can conclude that the (C^N)Pt(acac) complexes based on 2-phenylbenzoimidazole derivatives and acac ligands satisfy the need of the platinum(II) complexes as high efficient phosphorescent materials, in which emitting core or central

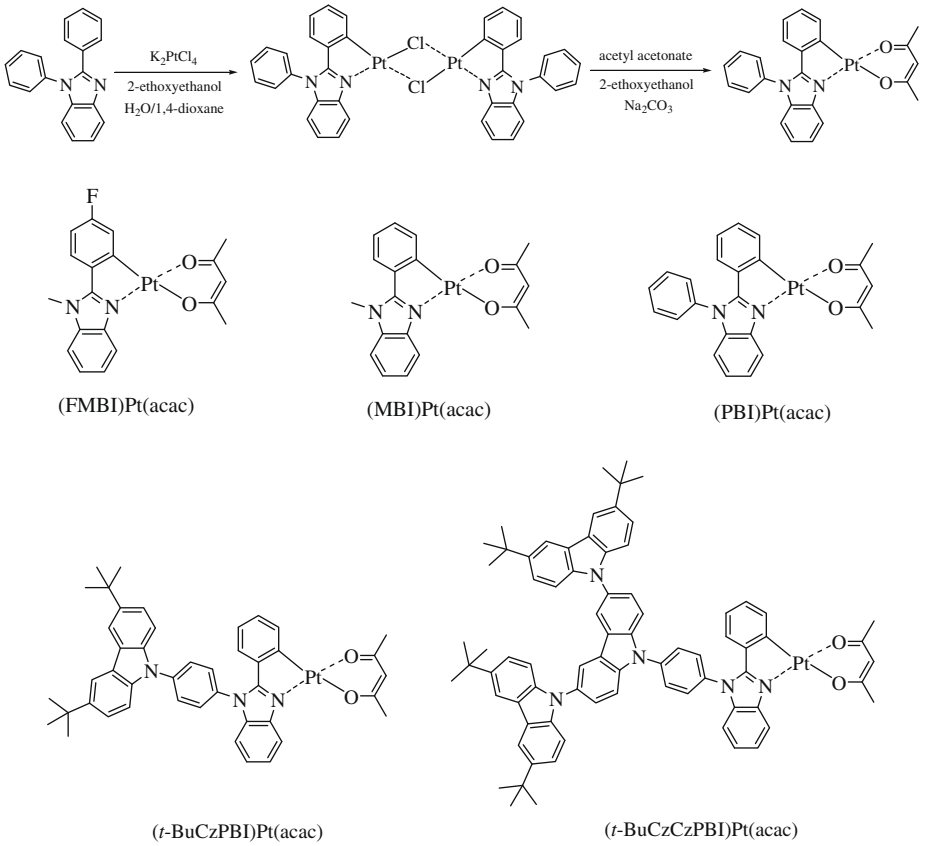

Scheme 1. Synthesis of the (C^N)Pt(acac) complexes with (PBI)Pt(acac) as an example (top) and molecular structures of the (C^N)Pt(acac) (bottom).

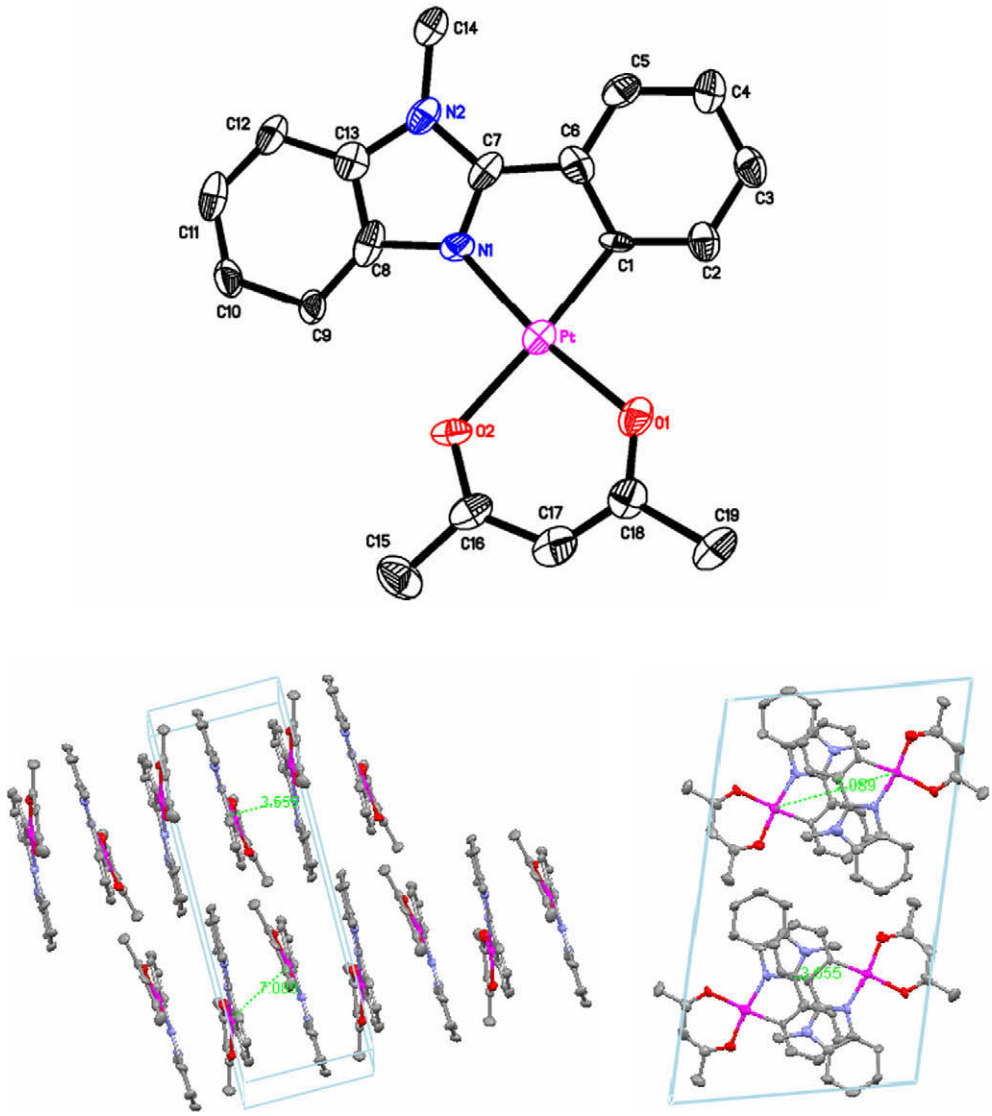

Fig. 1. ORTEP drawing of (MBI)Pt(acac) with thermal ellipsoids representing a 50% probability limit (top) and crystal packing diagram of (MBI)Pt(acac) (bottom) (hydrogen atoms have been omitted for clarity).

Table 1
Selected structure parameters for complex (MBI)Pt(acac).

Bond lengths (Å)			
Pt–C(1)	1.973(1)	Pt–O(1)	1.990(9)
Pt–N(1)	2.000(1)	Pt–O(2)	2.049(9)
Bond angles (°)			
C(1)–Pt–O(1)	91.7(4)	C(1)–Pt–N(1)	80.1(4)
O(1)–Pt–O(2)	92.5(4)	N(1)–Pt–O(2)	95.7(4)
C(1)–Pt–O(2)	175.7(1)	C(1)–Pt–O(1)	171.0(6)
Torsion angles (°)			
C(1)–C(6)–C(7)–N(1)	2.58	N(1)–C(8)–C(13)–C(12)	0.75
Dihedral angles (°)			
The planes of PtC(1)C(6)C(7)N(1) and PtO(1)O(2)C(16)C(17)C(18)			5.0

coordination unit around Pt atom should maintain a plane as possible.

There are four independent molecules in each cell unit, which are divided into two pairs. The parts of 2-phenylbenzoimidazole in each pair pack by the way of head-to-tail with intermolecular spacing of 3.55 Å that is longer than other reported platinum(II) complexes [15,51]. It shows, although the existence of π–π interaction between the adjacent molecules means the formation of aggregates or excimers, its possibility becomes weak at some degree in this kind of asymmetric molecule. The shortest metal to metal distance is 7.09 Å, proving no Pt–Pt interaction exists.

2.2. Photophysical properties characterization

Fig. 2 shows the absorption spectra of the (C^N)Pt(acac) complexes in CH_2Cl_2 solution with the concentration of 10^{-5} M at room temperature, and the absorption maxima and intensities of the absorption bands are listed in Table 2. Compared with the absorption spectra of the free ligands, a vibronic progression feature of these complexes in the short wavelength region (230–314 nm) is commonly assigned to the spin-allowed singlet π–π* intraligand transitions (^{1}IL) [8]. The weak, broad band with the small molar extinction coefficient (10^3, Table 2) located in the long wavelength region (400 nm) is attributed to the transition of the mixing state incorporating the ^{3}MLCT and the ^{3}IL [52,53], and the absorption bands located at 351–370 nm can be ascribed the ^{1}MLCT. The existence of the mixed state ^{1}MLCT and ^{3}MLCT due to the strong spin–orbit coupling induced by the platinum heavy atom, according to

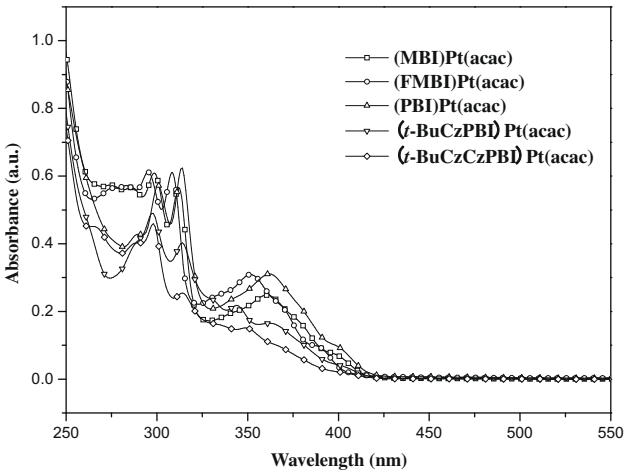

Fig. 2. The UV–Vis absorption spectra of the (C^N)Pt(acac) complexes in CH_2Cl_2 with the concentration of 10^{-5} M at room temperature.

other published platinum(II) complexes, such as (ppy)Pt(acac) [15], indicates that these (C^N)Pt(acac) complexes are typical phosphorescent materials. As for the absorption peak at 332, 344 and 333, 349 nm in the spectra of (*t*-BuCzPBI)Pt(acac) and (*t*-BuCzCzPBI)Pt(acac), they should be ascribed to the carbazole groups [46]. The introduction of electron-withdrawing fluorine atoms on the phenyl ring gives a marked 11 nm blue shift at 350–370 nm for (FMBI)Pt(acac), while the absorbance peak of (PBI)Pt(acac) containing aromatic substituent only red-shifts 1–2 nm, comparing to (MBI)Pt(acac). Interestingly, as the conjugated π system of the C^N ligand increases, the absorption wave of (*t*-BuCzPBI)Pt(acac) and (*t*-BuCzCzPBI)Pt(acac) are nearly identical except the intensity weaker.

The PL spectra of the (C^N)Pt(acac) complexes both in CH_2Cl_2 solution and the film are showed in Fig. 3. The emissive data are also included in Table 2. All of the complexes have two emissions maxima in the range of 480–530 nm (Fig. 3, top) together with a shoulder, which is produced by aggregates. They are typical green phosphorescent materials and possess high phosphorescence quantum yields ranging from 0.08 to 0.17 in solutions at room temperature. With (MBI)Pt(acac) as reference, the emission maximum of (FMBI)Pt(acac) blue-shifts about 9 nm because of the presence of electron-withdrawing substituent group (F). In contrast, (PBI)Pt(acac) exhibits a red shift of 7 nm due to the extension of π conjugation of ligands. The emission maxima of (PBI)Pt(acac), (*t*-BuCzPBI)Pt(acac) and (*t*-BuCzCzPBI)Pt(acac) are 494 and 527, 498 and 530, and 500 and 532 nm, respectively. The PL profiles of the three complexes are identical except the peak position having a small red shift below 5 nm. This illuminates that connecting the carbazole dendrons to the (PBI)Pt(acac) does not change the optical properties obviously.

The film PL spectra are also characterized in order to investigate the possible stacking effects of the planar platinum(II) complexes. It is worth noting that the film PL spectrum of (MBI)Pt(acac) is almost the same as that in solution (Fig. 3, bottom, inset), indicating that the stacking effect is too small to affect any associated photophysical behavior. Although there is a weak shoulder peak at 560 nm attributed to the emission of excimers produced by weak π–π interaction no matter in solution or film, it can still testify that 2-phenylbenzoimidazole C^N ligand is a suitable cyclometalated ligand for the planar platinum(II) complexes. In contrary, the film PL spectra of (FMBI)Pt(acac) and (PBI)Pt(acac) become broader and the shoulder peaks go into stronger. What's more, the film PL spectrum of (PBI)Pt(acac) only displays one broad peak. It may result from the effect of strong electronegative fluorine atom and plane benzene ring, which strengthen the intermolecular interaction. Compared with (PBI)Pt(acac), the film PL spectra of (*t*-BuCzPBI)Pt(acac) and (*t*-BuCzCzPBI)Pt(acac) with the bulky and rigid *t*-butylcarbazole show subtle vibronic structures as well as the disappearance of the shoulder peaks despite a slightly red shift. It accounts for the encumbrance among dendrons of *t*-butylcarbazole restraining the excimers formation successfully in the nature of things. Therefore the carbazole dendrons mainly act as a bulky and rigid group to separate the emissive cores from each other and suppress aggregates of the molecules of platinum(II) complexes. Naturally, phosphorescence quantum yields of the two complexes (Table 2) gradually increase in comparison with (PBI)Pt(acac).

2.3. Electrochemical properties characterization

The electrochemical properties of these complexes were performed using cyclic voltammetry (CV) and the redox data are shown in Table 2. To understand their electronic structures qualitatively, DFT calculations were performed on complex (MBI)Pt(acac) using DFT-B3LYP [54] coupled to LANL2DZ basis set [55] including some relativistic effects, which have been used successfully for other planar platinum(II) complexes [15–18]. The spatial plots used for the ground state calculations based on crystal structure are given in Fig. 4.

All the complexes displayed oxidation waves in dichloromethane and no reduction waves were detected. The Pt(II) redox pro-

Table 2
Photophysical and electrochemical performance of the (C^N)Pt(acac) complexes.

Complexes	λ_{abs}[a] (log ε) (nm)	λ_{em}[a] (nm) [τ (μs)][c]	λ_{em}[b] (nm) [τ (μs)][d]	φ_P[a]	HOMO[e] (eV)	LUMO[e] (eV)	ΔE[f] (eV)
(FMBI)Pt(acac)	245 (4.7), 276 (4.5), 283 (4.5), 295 (4.5), 308 (4.5), 351 (4.2), 390 (3.7)	478, 513 [0.61]	478, 513 [0.13]	0.08	−5.03	−1.95	3.08
(MBI)Pt(acac)	248 (4.9), 276 (4.6), 286 (4.6), 298 (4.6), 312 (4.6), 360 (4.3), 400 (3.7)	487, 523 [5.84]	487, 523 [0.13]	0.10	−5.00	−2.03	2.97
(PBI)Pt(acac)	230 (4.8), 247 (4.7), 288 (4.4), 300 (4.5), 313 (4.6), 362 (4.3), 401 (3.7)	494, 527 [6.65]	548 [0.64]	0.14	−5.05	−2.09	2.96
(*t*-BuCzPBI)Pt(acac)	230 (4.9), 243 (4.9), 288 (4.5), 297 (4.6), 314 (4.5), 332 (4.3), 344 (4.3), 362 (4.1), 404 (3.5)	498, 530 [6.64]	511, 540 [0.97]	0.16	−5.06	−2.11	2.95
(*t*-BuCzCzPBI)Pt(acac)	241 (5.3), 266 (4.9), 288 (4.9), 298 (4.9), 314 (4.7), 333 (4.2), 349 (4.4), 370 (4.2), 405 (3.5)	500, 532 [7.54]	516, 542 [1.21]	0.17	−5.08	−2.13	2.95

[a] Measured in CH_2Cl_2 solution with the concentration of 10^{-5} M at room temperature.
[b] Measured in the film state at room temperature.
[c] Measured in degassed CH_2Cl_2 solution with the concentration of 10^{-5} M at room temperature; the excitation wavelength was set at 355 nm.
[d] Measured in the film state at room temperature; the excitation wavelength was set at 355 nm.
[e] Measured in CH_2Cl_2 at room temperature with 0.1 mol dm^{-3} *n*-Bu_4NClO_4 as supporting electrolyte; scanning rate: 100 mV s^{-1}; values are reported vs. Fc^+/Fc.
[f] ΔE = LUMO−HOMO.

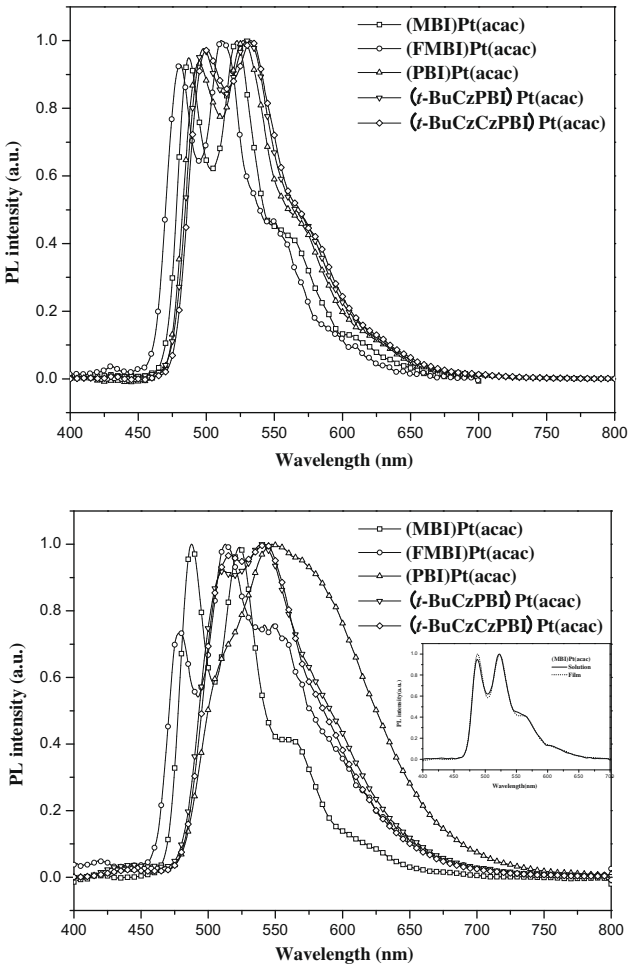

Fig. 3. The photoluminescence (PL) spectra of the (C^N)Pt(acac) complexes in CH_2Cl_2 solution with the concentration of 10^{-5} M (top) and the spin-coating film (bottom) at room temperature. The inset shows solution (CH_2Cl_2, 10^{-5} M) and film PL spectra of (MBI)Pt(acac).

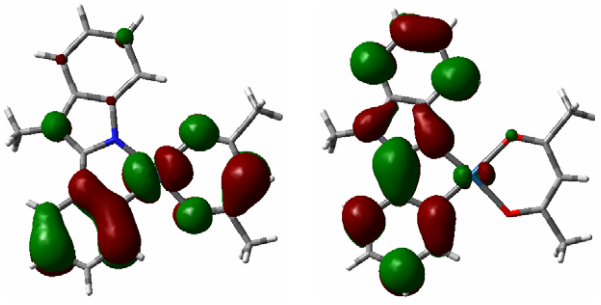

Fig. 4. Density functional theory (DFT) calculation of HOMO (left) and LUMO (right) for (MBI)Pt(acac).

cesses are usually irreversible, not like the Pt(I) and Pt(III) [56]. In accordance with literatures [15], the HOMO mainly consists of d-orbitals from Pt center mixing with the π-orbitals of both the phenyl ring and acetyl acetonate ligand that are directly bonded to the Pt center. And the LUMO is related to the π^* orbitals of the 2-phenylbenzoimidazole ligand (Fig. 4). The HOMO and LUMO energy levels (Table 2) were calculated from CV data together with absorption spectra. In general, the electron-donating substituent group raises the HOMO orbitals, and the LUMO orbitals are the reverse truth for an electron-withdrawing substituent group [57,58]. By comparing with (MBI)Pt(acac) (HOMO: −5.00 eV; LUMO: −2.03 eV), the HOMO level of (FMBI)Pt(acac) reduces about 0.03 eV, due to the introduction of electron-withdrawing fluorine atom. And extension of ligand π conjugation leads to a lower LUMO level for (PBI)Pt(acac) (−2.09 eV). Consistent with carbazole-based iridium dendrimers [46], both the HOMO and LUMO levels gradually decreases in the sequence of (PBI)Pt(acac), (*t*-BuCzPBI)Pt(acac) and (*t*-BuCzCzPBI)Pt(acac) with increasing dendron generation.

2.4. Electrophosphorescent properties characterization

The electroluminescent properties of these Pt(II) complexes were tested with a device configuration as shown in Fig. 5. The other organic materials used in this study were also shown in Fig. 5 including hole-transporting material of *N*,*N*′-di-1-napthyl-*N*,*N*′-diphenylbenzidine (NPB), host material of 4,4′-(*N*,*N*′-dicarbazole)biphenyl (CBP), exciton-blocking material of 2,9-dimethyl-4,7-diphenyl-1,10-phenanthroline (BCP) and electron-transporting material of tris(8-quinolinato) aluminium (Alq_3). (MBI)Pt(acac) and (PBI)Pt(acac) were tested with a device structure of ITO/NPB(50 nm)/CBP:Pt(wt.%)(30 nm)/BCP(10 nm)/Alq_3(40 nm)/LiF(1 nm)/Al since they can be easily deposited via thermal evaporation. For (*t*-BuCzPBI)Pt(acac) and (*t*-BuCzCzPBI)Pt(acac), they were tested with a device structure of ITO/PEDOT:PSS(50 nm)/CBP:Pt(wt.%)(30 nm)/BCP(15 nm)/Alq_3(40 nm)/LiF(1 nm)/Al via solution spin-coating. For comparison, the device of (PBI)Pt(acac) was also fabricated by solution-processible method. The device performances for these materials were listed in Table 3.

The electroluminescence (EL) spectra of the complexes are independent of the applied voltages from 6 to 16 V. Fig. 6 shows the EL spectra of the (C^N)Pt(acac) complexes at the driving voltage of 12 V. The EL spectra exhibit a 10–14 nm red shift of emission maximum compared to their PL spectra in solution, which may probably be attributed to the higher complexes concentration in devices and different environment. Gratifyingly, when doped into CBP host material, the EL spectrum of (PBI)Pt(acac) exhibits undiscerned shoulder emissions around 600 nm, which obviously appears in its film PL spectrum. It is worth noting that even at a high doping concentration of 30–40 wt.%, no discernable shoulder emissions around 600 nm are observed in their EL spectra as for (*t*-BuCzPBI)Pt(acac) and (*t*-BuCzCzPBI)Pt(acac). The fact demonstrates that the *t*-butylcarbazole dendrons can restrain the excimers formation and act as host material. The Commission Internationale de L'Eclairage (CIE) coordinates were calculated to be about (0.38, 0.56) for the (C^N)Pt(acac) complexes. The CIE coordinates of all the complexes are almost independent of driving voltages.

Fig. 7 shows the current density–voltage and brightness–voltage characteristics of the (C^N)Pt(acac) complexes based OLEDs. The turn-on voltage slightly increases for the solution-processed OLEDs compared with that of the thermally evaporation OLEDs. The brightnesses of all the (C^N)Pt(acac) complexes based OLEDs exceed 8000 cd/m^2 and the maximum brightnesses reach 13 605 and 13 608 cd/m^2 for the (MBI)Pt(acac) and (*t*-BuCzPBI)Pt(acac) based OLEDs, respectively. As shown in Fig. 8 and Table 3, the maximum luminous efficiencies are 15.1, 10.7, 17.5 and 9.2 cd/A, and the power efficiencies are 4.3, 4.8, 8.4 and 4.5 lm/W for the devices of (MBI)Pt(acac), (PBI)Pt(acac), (*t*-BuCzPBI)Pt(acac) and (*t*-BuCzCzPBI)Pt(acac), respectively. These results are comparable to those of other reported platinum(II) complexes derived from β-diketonate ligands [18,59].

The efficiency decay at high current densities and high doping concentrations resulting from triplet–triplet (T–T) annihilation is also observed for this class of mononuclear platinum(II) complexes based on 2-phenylbenzoimidazole derivatives [60,61]. However,

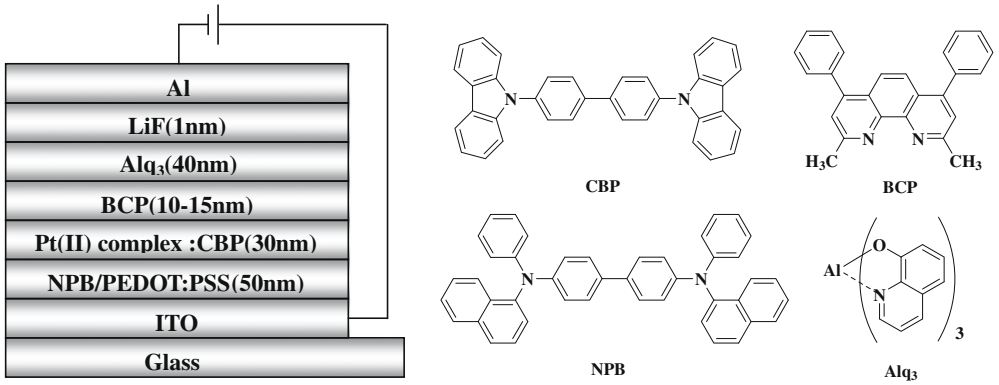

Fig. 5. Multilayer structure of the devices and the molecular structures of the complexes used in fabricating the EL devices.

Table 3
The electrophosphorescent performance of the devices using the (C^N)Pt(acac) complexes.

Complexes	Method	Turn-on voltage[a] (V)	Brightness[b] (cd m^{-2})	η_c[b] (cd A^{-1})	η_p[b] (lm W^{-1})	η_c[c] (cd A^{-1})	η_p[c] (lm W^{-1})	λ_{em}[b] (nm)	CIE at 12 V (x, y)
(MBI)Pt(acac) (12 wt.%)	Vacuum thermal evaporation	4.9	13 605	15.1	4.9	8.9	1.7	534	(0.38, 0.55)
(PBI)Pt(acac) (8 wt.%)		4.5	10 314	6.5	2.35	4.3	1.0	541	(0.38, 0.54)
(PBI)Pt(acac) (10 wt.%)	Solution spin-coating	6.2	11 123	10.7	4.8	6.8	2.0	540	(0.38, 0.56)
(*t*-BuCzPBI)Pt(acac) (10 wt.%)		6.0	5745	8.0	4.0	2.4	0.7	540	(0.35, 0.56)
(*t*-BuCzPBI)Pt(acac) (20 wt.%)		6.2	12 135	16.1	7.5	7.0	1.9	540	(0.38, 0.56)
(*t*-BuCzPBI)Pt(acac) (30 wt.%)		6.0	13 608	17.5	8.4	8.1	2.1	544	(0.39, 0.56)
(*t*-BuCzPBI)Pt(acac) (50 wt.%)		5.6	11 059	10.4	4.0	6.9	1.8	548	(0.40, 0.55)
(*t*-BuCzCzPBI)Pt(acac) (40 wt.%)		5.6	8251	9.2	4.5	4.6	1.2	544	(0.39, 0.56)

[a] At a brightness of 1 cd m^{-2}.
[b] At the maximum.
[c] At a current density of 100 mA cm^{-2}. η_c, luminous efficiency; η_p, power efficiency.

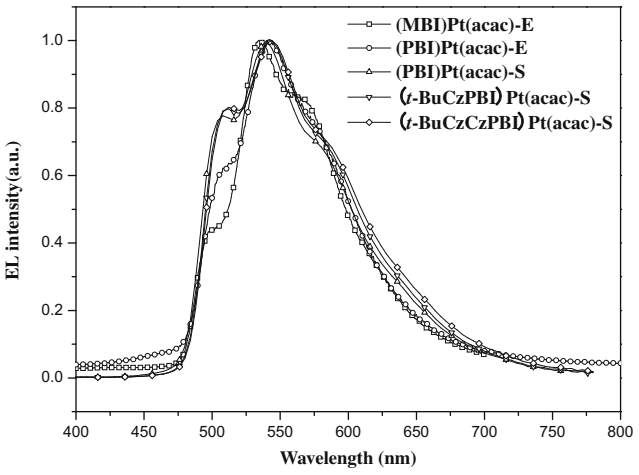

Fig. 6. EL spectra of the (C^N)Pt(acac) complexes at the driving voltage of 12 V. E, evaporation; S, solution.

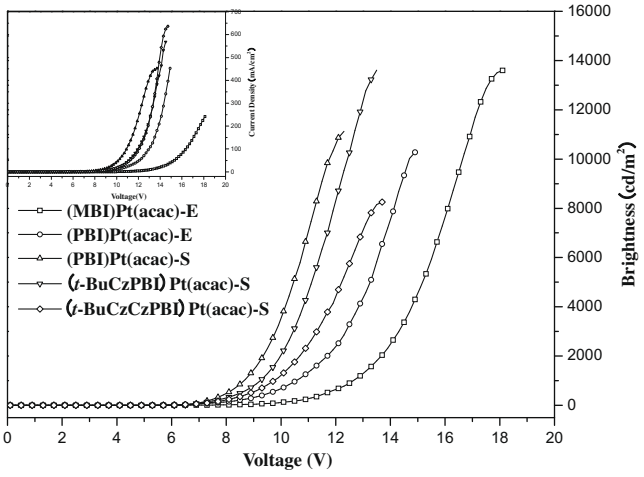

Fig. 7. Voltage and brightness characteristics for OLEDs using the (C^N)Pt(acac) complexes (inset: plot of current density vs. voltage). E, evaporation; S, solution.

even at a current density of 100 mA/cm^2, the luminous efficiency still remains as high as 8.9 cd/A for the (MBI)Pt(acac)-based device and 8.1 cd/A for the (*t*-BuCzPBI)Pt(acac)-based device, respectively, under the doping concentration of 30%. Overall, the high quality film, better square plane around of Pt atom center and inhibition function of *t*-butylcarbazole dendrons make them highly desirable as emissive dopant for phosphorescent OLEDs.

As shown in Table 3, the efficiency of high-vacuum thermal evaporation device is lower than that of the solution-processed device based on (PBI)Pt(acac). It may be due to crystallization during the process of thermal evaporation, which favors the T–T annihilation. In addition, the device efficiency of (*t*-BuCzCzPBI)Pt(acac) is not the best among the complexes, which is unexpected. We are suspicious of CBP host material having bad compatibility with (*t*-BuCzCzPBI)Pt(acac). More detail work for seeking suitable host material and optimizing the device performance of (*t*-BuCzCzPBI)Pt(acac) is ongoing in our group.

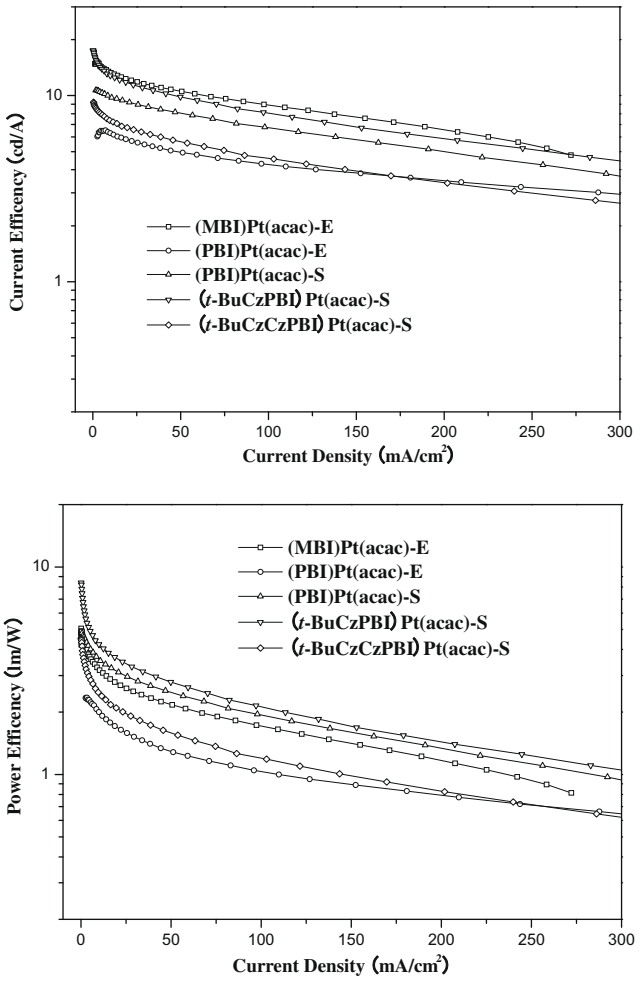

Fig. 8. Current density dependence of current efficiency (top) and power efficiency (bottom) of the (C^N)Pt(acac) complexes. E, evaporation; S, solution.

3. Conclusions

In summary, we have synthesized and characterized five neutral square planar platinum(II) complexes based on 2-phenylbenzoimidazole derivative ligands. They are easily prepared and stable in air. X-ray structure analysis of (MBI)Pt(acac) demonstrates that 2-phenylbenzoimidazole is a suitable ligand for constructing Pt complexes with ideal coordination geometry combined with acac anion. These complexes exhibit green phosphorescence at room temperature with high quantum efficiency. Introduced bulky and rigid carbazole-based dendrons, which can restrain the formation of aggregates and excimers further improve luminous efficiency. Among the five complexes, (MBI)Pt(acac) and (*t*-BuCzPBI)Pt(acac) show the best device performance with a peak luminous efficiency of 15.1 and 17.5 cd/A based on thermal evaporation and solution-processed OLED devices, respectively. All these features indicate the five platinum(II) complexes are promising candidates for efficient green OLEDs.

4. Experimental

4.1. General remarks

4.1.1. Materials

All chemicals and reagents for chemical synthesis were used as received from commercial sources without further purification. Some solvents, such as dichloromethane (DCM), tetrahydrofuran (THF), toluene were purified following the standard procedures just before used as characterization. The ligands H-FMBI, H-MBI, H-PBI, *t*-BuCz-H-PBI and *t*-BuCzCz-H-PBI were prepared according to the literature procedures [62–64]. All reactions were carried out in a dry argon atmosphere.

4.1.2. Physical measurements

The UV–Vis spectra and photoluminescence (PL) spectra were measured by Perkin–Elmer Lambda 35 UV–Vis spectrometer and Perkin–Elmer LS 50B spectrofluorometer at room temperature in aerated dichloromethane, respectively. The solution PL quantum efficiencies were measured and calculated by a relative method using (ppy)Pt(acac) (Φ_{em} = 0.15 in dichloromethane) as a Ref. [63]. Cyclic voltammetry experiments were performed on an EG&G 283 (Princeton Applied Research) potentiostat/galvanostat system. All measurements were carried out at room temperature with a conventional three-electrode system consisting of a platinum working electrode, a platinum counter electrode and an Ag/AgCl reference electrode. The supporting electrolyte was 0.1 M tetrabutylammonium perchlorate (n-Bu_4NClO_4). The ferrocene was used as a standard to calibrate the system. The scan rate was 100 mV s^{-1}. ^1H and ^{13}C NMR spectra were recorded on Bruker AV 300 spectrometers and referenced to TMS as an internal standard. Elemental analyses were carried out using a Bio-Rad Co's elemental analytical instrument. Thermal gravimetric analysis (TGA) was performed under a flow of nitrogen at a heating rate of 10 °C/min with Perkin–Elmer-TGA 7 thermal gravimetric analyzer. MALDI/TOF mass spectra were obtained on an AXIMA CFR MS apparatus (COMPACT). The experimental error is estimated to be ±10%.

4.2. Preparations of platinum(II) complexes

4.2.1. General procedure for preparation of platinum(II) complexes

The Pt(II) μ-dichloro-bridged dimers were synthesized following a modified method of Lewis [65]. This involves heating the K_2PtCl_4 salt with 2.05 equiv. of 2-phenylbenzoimidazole derivatives in a 3:1 mixture of 2-ethoxyethanol and water to 80 °C for 16–72 h, which resulted in a green-yellow coloured dimer that was distinctly discernable from the mixture. The precipitate was collected by filtration and washed with water and ethanol. After dried, the crude product was directly used for next step without further purification.

Then the chloro-bridged dimers, 3–10 equiv. of the acetyl acetonate and 10 equiv. of Na_2CO_3 in 2-ethoxyethanol were refluxed 16–48 h before cooled to room temperature. The mixture was poured into water for extraction with dichloromethane. The organic extracts were washed with water and dried over anhydrous sodium sulfate. After the solvent was completely removed, the residue was purified by column chromatography on silica gel with dichloromethane/petroleum (1:1) as the eluent to afford pure product with the yield in rang of 11–66%.

4.2.2. Structure characterization of platinum(II) complexes

(MBI)Pt(acac): yield: 41%. ^1H NMR (300 MHz, DMSO-d_6, ppm): δ 8.34 (t, J = 4.5 Hz, 1H), 7.79–7.74 (m, 2H), 7.55 (d, J = 8.79 Hz, 1H), 7.41–7.39 (m, 2H), 7.16–7.14 (m, 2H), 5.64 (s, 1H), 2.03 (s, 3H), 1.95 (s, 3H).

(FMBI)Pt(acac): yield: 11%. ^1H NMR (300 MHz, DMSO-d_6, ppm): δ 8.29 (d, J = 4.5 Hz, 1H), 7.85–7.80 (m, 1H), 7.73 (d, J = 8.34 Hz, 1H), 7.39–7.34 (m, 2H), 7.16 (dd, J = 10.52, 2.37 Hz, 1H), 6.95 (t, J = 8.57 Hz, 1H), 5.64 (s, 1H), 2.02 (s, 3H), 1.95 (s, 3H).

(PBI)Pt(acac): yield: 66%. ^1H NMR (300 MHz, $CDCl_3$, ppm): δ 8.55 (d, J = 8.1 Hz, 1H), 7.72–7.67 (m, 4H), 7.53 (d, J = 3.3 Hz, 1H), 7.51 (d, J = 3.45 Hz, 1H), 7.38 (td, J = 7.7, 0.6 Hz, 1H), 7.26 (td, J = 8.1, 0.9 Hz, 1H), 7.09 (td, J = 8.25, 1.5 Hz, 1H), 7.01 (d, J = 8.1 Hz, 1H), 6.75 (td, J = 8.1, 0.9 Hz, 1H), 6.41 (d, J = 6.9 Hz,

1H), 5.54 (s, 1H), 2.09 (s, 3H), 2.01 (s, 3H). ^{13}C NMR (300 MHz, $CDCl_3$, ppm): δ 185.4, 183.7, 140.5, 139.3, 136.2, 135.2, 134.8, 131.1, 130.8, 130.7, 129.7, 128.5, 124.8, 124.5, 123.8, 123.2, 117.2, 110.8, 102.5, 28.3, 27.7. Anal. Calc. for $C_{24}H_{20}N_2O_2Pt$: C, 51.15; H, 3.58; N, 4.97. Found: C, 51.44; H, 3.70; N, 4.68%. MALDI-TOF (m/z): 563.1 [M^++H].

(t-BuCzPBI)Pt(acac): yield: 31%. ^{1}H NMR (300 MHz, $CDCl_3$, ppm): δ 8.86 (d, J = 8.1 Hz, 1H), 8.19 (S, 2H), 7.91 (d, J = 8.4 Hz, 2H), 7.76–7.74 (d, 3H), 7.55 (S, 4H), 7.43 (t, J = 7.2 Hz, 1H), 7.34 (t, J = 7.7 Hz, 1H), 7.18 (d, J = 7.8 Hz, 1H), 7.15 (t, J = 7.5 Hz, 1H), 6.86 (t, J = 7.1 Hz, 1H), 6.63 (d, J = 7.5 Hz, 1H), 5.56 (s, 1H), 2.11 (s, 3H), 2.03 (s, 3H), 1.50 (s, 18H). ^{13}C NMR (300 MHz, $CDCl_3$, ppm): δ 185.5, 183.8, 164.0, 144.2, 140.6, 139.5, 139.1, 136.2, 134.8, 133.0, 131.3, 130.1, 129.9, 128.3, 125.1, 124.4, 124.0, 123.4, 117.3, 117.0, 110.8, 109.5, 102.6, 35.2, 32.4, 28.3, 27.7. Anal. Calc. for $C_{44}H_{43}N_3O_2Pt$: C, 62.85; H, 5.15; N, 5.00. Found: C, 62.86; H, 5.27; N, 4.03%. MALDI-TOF (m/z): 840.3 [M^++H].

(t-BuCzCzPBI)Pt(acac): yield: 25%. ^{1}H NMR (300 MHz, $CDCl_3$, ppm): δ 8.64 (d, J = 8.1 Hz, 1H), 8.30 (d, J = 1.8 Hz, 2H), 8.18 (d, J = 1.5 Hz, 4H), 8.11 (d, J = 8.4 Hz, 2H), 7.91 (d, J = 8.4 Hz, 2H), 7.82 (d, J = 8.7 Hz, 2H), 7.78 (d, J = 7.5 Hz, 1H), 7.71 (dd, J = 8.6, 1.95 Hz, 2H), 7.50–7.43 (m, 5H), 7.40–7.35 (m, 5H), 7.24 (d, J = 7.2 Hz, 1H), 7.17 (td, J = 7.5, 1.2 Hz, 1H), 6.91 (td, J = 7.61, 1.2 Hz, 1H), 6.72 (d, J = 7.2 Hz, 1H), 5.58 (s, 1H), 2.13 (s, 3H), 2.04 (s, 3H), 1.47 (s, 36H). ^{13}C NMR (300 MHz, $CDCl_3$, ppm): δ 185.5, 183.8, 164.0, 143.2, 140.7, 140.5, 140.2, 139.7, 139.6, 136.1, 134.7, 134.3, 132.1, 131.4, 130.6, 130.1, 129.0, 126.7, 125.2, 125.0, 124.3, 124.2, 124.0, 123.6, 123.4, 120.0, 117.5, 116.7, 111.4, 110.7, 109.4, 102.6, 35.2, 32.5, 28.3, 27.7. Anal. Calc. for $C_{76}H_{73}N_2O_2Pt$: C, 71.12; H, 5.73; N, 5.46. Found: C, 70.29; H, 6.02; N, 4.24%. MALDI-TOF (m/z): 1283.7 [M^++H].

4.3. X-ray crystallographic studies for (MBI)Pt(acac)

Single crystals of (MBI)Pt(acac) were grown from dichloromethane/methanol solution at room temperature. A selected crystal was collected on a Bruker Smart APEX diffractometer with CCD detector and graphite monochromator, Mo Kα radiation (λ = 0.71073 Å). The intensity data were recorded with ω scan mode (187 K). Lorentz, polarization factors were made for the intensity data and absorption corrections were performed using SADABS program [66]. The crystal structure was solved using the SHELXTL program and refined using full matrix least squares [67]. The positions of hydrogen atoms were calculated theoretically and included in the final cycles of refinement in a riding model along with attached carbons.

C19H18N2O2Pt, MW = 501.44, yellowish green needles crystal, 0.33 × 0.22 × 0.06 mm^3, monoclinic, $P2_1/c$, a = 12.0577(16), b = 7.0243(9), c = 19.994(3) Å, β = 102.999(1), V = 1650.1(4) Å^3, Z = 4, $D_{calcd.}$ = 2.018 g/cm^3, μ = 8.517 mm^{-1}, R_1/wR_2 [$I > 2\sigma(I)$]: 0.0733/0.1922. R_1/wR_2 [all reflections]: 0.0842/0.2030. S = 1.080. Residual electron density: 9.365 and −3.507 e Å^{-3}.

4.4. Density functional calculations

DFT calculations were performed using GAUSSIAN 03W software package using a spin-restricted formalism at the B3LYP level. Popular 6-31G* (CNOH) was used to optimized the molecular geometry as basis set for all elements, and Los Alamos ECP plus DZ (LANL2DZ) was used for Pt as well. The HOMO and LUMO energies were determined using minimized singlet geometries to approximate the ground state.

4.5. OLEDs fabrication and characterization

The OLEDs were fabricated via thermal evaporation or spin-coating process for different Pt(II) complexes. An indium–tin-oxide (ITO) coated glass substrate was precleaned and subjected to UV-Ozone treatment for 25 min. For the thermally evaporation OLEDs, the organic layers were deposited in vacuum with a base pressure of 10^{-4} Pa with a sequence of a N,N'-di-1-napthyl-N,N'-diphenylbenzidine (NPB) hole-transport layer (50 nm), a 4,4′-(N,N'-dicarbazole)biphenyl (CBP): Pt(II) complex emitting layer (30 nm), a 2,9-dimethyl-4,7-diphenyl-1,10-phenanthroline (BCP) hole/exciton-block layer (10 nm) and a tris(8-quinolinato)aluminium (Alq_3) electron-transport layer (40 nm). Finally, a 10-Å-thick lithium fluoride (LiF) electron-injection layer and a 1000-Å-thick aluminum (Al) cathode were deposited. The light-emitting layer of CBP doped with Pt(II) complex were co-evaporated with two independent quartz crystal oscillators to monitor the doping ratio. For the solution-processed OLEDs, a 50-nm-thick PEDOT: PSS film replaced NPB as the hole-transport layer on ITO anode and was cured at 120 °C in air for 30 min. The emitting layer was then prepared by spin-coating a toluene solution of CBP and Pt(II) complex mixture at a concentration of 10 mg/ml and followed by drying at 65 °C in vacuum for 30 min. Subsequently, BCP, Alq_3, LiF, and Al were evaporated in vacuum. The active area of the diodes is 14 mm^2. The current-density–voltage and brightness–voltage curves of the devices were measured using a Keithley 2400 source meter and a PR650 spectra colorimeter. The EL spectra and CIE coordinates were recorded using the PR650 spectra colorimeter. All the experiments and measurements were carried out at room temperature under ambient conditions.

5. Supplementary material

CCDC 720936 contains the supplementary crystallographic data for (MBI)Pt(acac). These data can be obtained free of charge from The Cambridge Crystallographic Data Centre via www.ccdc.cam.ac.uk/data_request/cif.

Acknowledgements

This work is supported by the National Natural Science Foundation of China (Nos. 50673088 and 20874098), Science Fund for Creative Research Groups (No. 20621401) and 973 Project (No. 2009CB623600). The authors thank Professor Jingping Zhang (Faculty of Chemistry, Northeast Normal University, Changchun 130024, PR China) for her help in DFT calculations of the HOMO and LUMO for (MBI)Pt(acac).

References

[1] T.J. Wadas, Q.-M. Wang, Y.-J. Kim, C. Flaschenreim, T.N. Blanton, R. Eisenberg, J. Am. Chem. Soc. 126 (2004) 16841.
[2] M.G. Fisher, P.A. Gale, M.E. Light, S.J. Loeb, Chem. Commun. (2008) 5695.
[3] W.-Y. Wong, X.-Z. Wang, Z. He, A.B. Djurisic, C.-T. Yip, K.-Y. Cheung, H. Wang, C.K. Mak, W.-K. Chan, Nat. Mater. 6 (2007) 521.
[4] W.-Y. Wong, C.-L. Ho, Coord. Chem. Rev., doi:10.1016/j.ccr.2009.01.013.
[5] D.-L. Ma, C.-M. Che, S.-C. Yan, J. Am. Chem. Soc. 126 (2004) 16841.
[6] C.-M. Che, S.-C. Chan, H.-F. Xiang, M.C.W. Chan, Y. Liu, Y. Wang, Chem. Commun. (2004) 1484.
[7] T.W. Green, R. Lieberman, N. Mitchell, J.A.K. Bauer, W.B. Connick, Inorg. Chem. 44 (2005) 1955.
[8] R.C. Evans, P. Douglas, C.J. Winscom, Coord. Chem. Rev. 250 (2006) 2093.
[9] A.A. Rachford, S. Goeb, F.N. Castellano, J. Am. Chem. Soc. 130 (2008) 2766.
[10] V.N. Kozhevnikov, B. Donnio, D.W. Bruce, Angew. Chem., Int. Ed. 47 (2008) 1.
[11] J.A.G. Williams, S. Develay, D.L. Rochester, L. Murphy, Coord. Chem. Rev. 252 (2008) 2596.
[12] M.A. Baldo, D.F. O'Brien, Y. You, A. Shoustikov, S. Sibley, M.E. Tompson, S.R. Forrest, Nature 395 (1998) 151.
[13] W.B. Connick, L.M. Henling, R.E. Marsh, H.B. Gray, Inorg. Chem. 35 (1996) 6261.
[14] C.E. Whittle, J.A. Weinstein, M.W. George, K.S. Schanze, Inorg. Chem. 40 (2001) 4053.
[15] J. Brooks, Y. Babayan, S. Lamansky, P.I. Djurovich, I. Tsyba, R. Bau, M.E. Thompson, Inorg. Chem. 41 (2002) 3055.
[16] W.-Y. Wong, Z. He, S.-K. So, K.-L. Tong, Z. Lin, Organometallics 24 (2005) 4079.
[17] Z. He, W.-Y. Wong, X. Yu, H.-S. Kwok, Z. Lin, Inorg. Chem. 45 (2006) 10922.

[18] G.-J. Zhou, X.-Z. Wang, W.-Y. Wong, X.-M. Yu, H.-S. Kwok, Z. Lin, J. Organomet. Chem. 692 (2007) 3461.
[19] G.-J. Zhou, W.-Y. Wong, B. Yao, Z. Xie, L. Wang, J. Mater. Chem. 18 (2008) 1799.
[20] W.-Y. Wong, C.-L. Ho, J. Mater. Chem. (2009), doi:10.1039/d819943d.
[21] Y.-Y. Lin, S.-C. Chan, M.C.W. Chan, Y.-J. Hou, N. Zhu, C.-M. Che, Y. Liu, Y. Wang, Chem. Eur. J. 9 (2003) 1264.
[22] D.R. McMillin, J.J. Moore, Coord. Chem. Rev. 229 (2002) 113.
[23] L.J. Grove, J.M. Rennekamp, H. Jude, W.B. Connick, J. Am. Chem. Soc. 126 (2004) 1594.
[24] W. Lu, N. Zhu, C.-M. Che, Chem. Commun. (2002) 900.
[25] K.-H. Wong, M.C.W. Chan, C.-M. Che, Chem. Eur. J. 5 (1999) 2845.
[26] C.-M. Che, W.-F. Fu, S.-W. Lai, Y.-J. Hou, Y.-L. Liu, Chem. Commun. (2003) 118.
[27] C.-M. Che, J.-L. Zhang, L.-R. Lin, Chem. Commun. (2002) 2556.
[28] D.-L. Ma, C.-M. Che, Chem. Eur. J. 9 (2003) 6133.
[29] W. Lu, M.C.W. Chan, N. Zhu, C.-M. Che, C. Li, Z. Hui, J. Am. Chem. Soc. 126 (2004) 7639.
[30] W. Lu, B.-X. Mi, M.C.W. Chan, Z. Hui, C.-M. Che, N. Zhu, S.-T. Lee, J. Am. Chem. Soc. 126 (2004) 4958.
[31] D.F. Qiu, J. Wu, Z.Y. Xie, Y.X. Cheng, L.X. Wang, J. Organomet. Chem. 694 (2009) 737.
[32] C.-C. Kwok, H.M.Y. Ngai, S.-C. Chan, I.H.T. Sham, C.-M. Che, N. Zhu, Inorg. Chem. 44 (2005) 4442.
[33] W. Sotoyama, T. Satoh, N. Sawatari, H. Inoue, Appl. Phys. Lett. 86 (2005) 153505.
[34] X. Yang, Z. Wang, S. Madakuni, J. Li, G.E. Jabbour, Adv. Mater. 20 (2008) 2405.
[35] T.K. Aldridge, E.M. Stacy, D.R. McMillin, Inorg. Chem. 33 (1994) 722.
[36] V.M. Miskowski, V.H. Houlding, C.-M. Che, Y. Wang, Inorg. Chem. 32 (1993) 2518.
[37] J.A.G. Williams, A. Beeby, E.S. Davies, J.A. Weinstein, C. Wilson, Inorg. Chem. 42 (2003) 8609.
[38] S.T.F. Kui, I.H.T. Sham, C.C.C. Cheung, C.-W. Ma, B. Yan, N. Zhu, C.-M. Che, W.-F. Fu, Chem. Eur. J. 13 (2007) 417.
[39] C.-W. Chan, T.-F. Lai, C.-M. Che, S.-M. Peng, J. Am. Chem. Soc. 115 (1993) 11245.
[40] B.W. Ma, P.I. Djurovich, M.E. Thompson, Coord. Chem. Rev. 249 (2006) 1501.
[41] J. Kavitha, Y. Chi, J.-K. Yu, S.-M. Peng, Y.-T. Tao, C.-H. Chien, A.J. Carty, Adv. Funct. Mater. 15 (2005) 223.
[42] Q.-D. Liu, W.-L. Jia, G. Wu, S. Wang, Organometallics 22 (2003) 3781.
[43] H. Jude, J.A.K. Bauer, W.B. Connick, Inorg. Chem. 44 (2004) 1211.
[44] B. Ma, J. Li, P.I. Djurovich, M. Yousuddin, R. Bau, M.E. Thompson, J. Am. Chem. Soc. 127 (2005) 28.
[45] B. Ma, P.I. Djurovich, S. Garon, B. Alleyne, M.E. Thomoson, Adv. Funct. Mater. 16 (2006) 2438.
[46] J.Q. Ding, J. Gao, Y.X. Cheng, Z.Y. Xie, L.X. Wang, D.G. Ma, X.B. Jing, F.S. Wang, Adv. Funct. Mater. 16 (2006) 575.
[47] H. Katoh, K. Miki, Y. Kai, N. Tanaka, N. Kasai, Chem. Soc. Jpn. 54 (1981) 611.
[48] A.C. Stückl, U. Klement, K.-J. Range, Z. Kristallogr. 208 (1993) 297.
[49] T.J. Giordano, P.G. Rasmussen, Inorg. Chem. 14 (1975) 1628.
[50] M. Ghedini, D. Pucci, A. Crispini, G. Barberio, Organometallics 18 (1999) 2116.
[51] M. Cocchi, D. Virgili, C. Sabatini, V. Fattori, P.D. Marco, M. Maestri, J. Kalinowski, Synthetic Met. 147 (2004) 253.
[52] J.Q. Ding, J. Gao, Q. Fu, Y.X. Cheng, D.G. Ma, L.X. Wang, Synthetic Met. 155 (2005) 539.
[53] I.R. Laskar, S.-F. Hsu, T.-M. Chen, Polyhedron 24 (2005) 881.
[54] A.D. Becke, J. Chem. Phys. 98 (1993) 5648.
[55] T.H. Dunning Jr., P.J. Hay, in: H.F. Schaefer III (Ed.), Modern Theoretical Chemistry, vol. 3, Plenum, New York, 1976, p. 1.
[56] P.-I. Kvam, M.V. Puzyk, K.P. Balashev, J. Songstad, Acta Chem. Scand. 49 (1995) 335.
[57] R. Pohl, J. Pavel Anzenbacher, Org. Lett. 5 (2002) 2769.
[58] R. Pohl, V.A. Montes, J. Shinar, J.P. Anzenbacher, J. Org. Chem. 69 (2004) 1723.
[59] C. Yang, X. Zhang, H. You, L. Zhu, L. Chen, L. Zhu, Y. Tao, D. Ma, Z. Shuai, J. Qin, Adv. Funct. Mater. 17 (2007) 651.
[60] C. Adachi, M.A. Baldo, S.R. Forrest, S. Lamansky, M.E. Thompson, R.C. Kwong, Appl. Phys. Lett. 78 (2001) 1622.
[61] C. Adachi, R. Kwong, S.R. Forrest, Org. Electron. 2 (2001) 37.
[62] F.A. Neugebauer, H. Fisher, S. Bamberger, H.O. Smith, Chem. Ber. 105 (1972) 2686.
[63] N.D. McClenaghan, R. Passalacqua, F. Loiseau, S. Campagna, B. Verheyde, A. Hameurlaine, W. Dehaen, J. Am. Chem. Soc. 125 (2003) 5356.
[64] W.-S. Huang, J.T. Lin, C.-H. Chien, Y.-T. Tao, S.-S. Sun, Y.-S. Wen, Chem. Mater. 16 (2004) 2480.
[65] B.N. Cockburn, D.V. Howe, T. Keating, B.F.G. Johnson, J. Lewis, J. Chem. Soc., Dalton Trans. (1973) 404.
[66] R.H. Blessing, Acta Crystallogr. A 51 (1995) 33.
[67] G.M. Sheldrick, SHELXTL, Version 5.1, Bruker Analytical X-ray Systems, Inc., Madison, WI, 1997.